Facile synthesis of photolabile dendritic-unit-bridged hyperbranched graft copolymers for stimuli-triggered topological transition and controlled release of Nile red

Journal:	*Polymer Chemistry*
Manuscript ID:	PY-ART-01-2015-000132.R1
Article Type:	Paper
Date Submitted by the Author:	07-Mar-2015
Complete List of Authors:	Zhao, Youliang; Soochow University, College of Chemistry, Chemical Engineering and Materials Science Mo, Bin; Soochow University, Liu, Huanhuan; Soochow University, Zhou, Xiangdong; Soochow University,

Cite this: DOI: 10.1039/c0xx00000x

www.rsc.org/xxxxxx

ARTICLE TYPE

Facile synthesis of photolabile dendritic-unit-bridged hyperbranched graft copolymers for stimuli-triggered topological transition and controlled release of Nile red†

Bin Mo,[a] Huanhuan Liu,[a] Xiangdong Zhou[b] and Youliang Zhao*[a]

Received (in XXX, XXX) Xth XXXXXXXXX 20XX, Accepted Xth XXXXXXXXX 20XX
DOI: 10.1039/b000000x

Different from hyperbranched starlike polymers and dendritic brushes, dendritic-unit-bridged hyperbranched graft copolymers (DHGCs) with branching point linked branches and linear grafts can be regarded as a new subclass of hyperbranched-*graft*-linear copolymers. This study aims at synthesis and properties of photocleavable DHGCs comprising oligomeric branches composed of poly(ethylene glycol) methyl ether acrylate (PEGA) units, linear poly(ε-caprolactone) (PCL) grafts and *o*-nitrobenzyl ester (ONBE) moieties in the dendritic unit. Based on a multifunctional inimer 3-((2-acryloyloxymethyl-2-hydroxymethyl)propionyloxy)methyl-2-nitrobenzyl 4-cyano-4-(phenylcarbonothioylthio)pentanoate (ANCP), functional DHGCs were controllably synthesized via two step reactions. RAFT copolymerization afforded hyperbranched poly(ANCP-*co*-PEGA) (PAP), and followed by CL polymerization to achieve PAP-*g*-PCL. Upon photo-cleavage, hyperbranched PAP was converted into linear polymers, and PAP-*g*-PCL was readily degraded into mixtures of linear, star and graft polymers. With increasing UV irradiation time, the PAP-*g*-PCL micelles were gradually evolved into vesicles and multicompartment vesicles due to photo-triggered cleavage and reaggregation. Upon normal and on-demand UV irradiation, the release kinetics for controlled release of Nile red from copolymer aggregates could be tuned in a wide range, revealing the great potential in smart drug delivery systems. This study affords a versatile method to construct photolabile DHGCs, which opens up a new route to explore unique properties of novel topological copolymers.

In polymer science, hyperbranched polymer has become an established subclass of dendritic macromolecules with multipurpose applications.[1–9] The synthesis can be usually achieved by one step reaction involving self-condensing vinyl polymerization (SCVP),[10–22] leading to the target highly branched polymers with controlled molecular weight, adjustable degree of branching and variable polydispersity. Owing to the potential in construction of versatile macromolecular architectures with hybrid structures, design and modification of hyperbranched polymers with other functional building blocks to form hyperbranched graft copolymers (HGCs) have attracted increasing interest recently.[4,5] The conjugation of different modules can not only maintain the feature of branching effect in physicochemical properties but introduce increasingly tunable functions such as stimuli-responsiveness, heterofunctionality, and biodegradability.[4,5,23–38] Thus far, various HGCs such as hyperbranched-*graft*-hyperbranched (HGHCs),[23–25] linear-*graft*-hyperbranched (LGHCs),[26–32] and hyperbranched-*graft*-linear (HGLCs) copolymers[13,14,33–38] have been successfully achieved. According to the location of linear blocks, HGLCs can be classified into three types, in which the linear segments can be grafted onto either the chain end to form starlike copolymers with a branched core,[33–36] the side chain of each branch to achieve dendritic brushes[13,14,37] or star polymers,[35,38] or the branching point to generate dendritic-unit-bridged HGCs (DHGCs). Although some star polymers and dendritic brushes have been synthesized,[13,14,33–38] no examples of DHGCs are available until now. At present, it is timely to explore the easy synthetic routes and potentially unique properties of these copolymers.

On the other hand, stimuli-sensitive polymers have attracted much attention since they can exhibit sharp responses to the environmental changes. Among them, light is regarded as the most elegant and non-invasive trigger that is easy to manipulate in a spatiotemporal manner and insusceptible to physiological parameters such as temperature, pH and ionic strength.[39–49] More recently, increasing emphasis has been paid on photosensitive polymers especially photocleavable polymers (PCPs). PCPs are liable to degrade into lower molecular weight fragments upon light irradiation, and they can hold great promise for applications in many fields including drug and gene delivery,[50–58] nanocage,[59] nanoporous thin film,[60–63] and micropattern.[64–66] With the introduction of metastable photochromic moieties, PCPs can be subjected to photo-triggered degradation as the functionalities are cracked from the building blocks. Linear PCPs can be usually classified into three types, namely, main-chain, side-chain and in-chain (with cleavable moiety at the block junction) structures.[39–41] For PCPs comprising hyperbranched polymers and HGCs, however, the classifications are more complex due to the

presence of multiple modules involving end groups, branching points, branches and grafted chains, in which the photolabile linkages can be located in all these building blocks. Among photosensitive groups, *o*-nitrobenzyl (ONB) alcohol derivative is a popular irreversible photolabile species, in which the photoisomerization from *o*-nitrobenzyl to *o*-nitrosobenzaldehyde can be rapidly conducted upon UV light irradiation.[67–69] The current researches primarily focus on linear polymers, and the examples on hyperbranched[53,66] and star[70] polymers with ONB moieties are relatively scarce. With introduction of various functionalities, the photolabile copolymers can potentially exhibit some unique properties such as disassembly, reassembly, and self-crosslinking besides self-immolative property.[53,54] As far as photocleavable hyperbranched polymers and their derivatives are concerned, light irradiation can induce dynamic degradation and lead to versatile topological transition, and they have a great potential in smart materials. With the rapid development of materials science, it is extremely urgent to construct these functional polymers and explore photo-tunable self-assembly behaviors and drug release properties.

This study aims at facile synthesis and properties of novel photocleavable DHGCs. To this end, an ONB-bearing inimer 3-((2-acryloyloxymethyl-2-hydroxymethyl)propionyloxy)methyl-2-nitrobenzyl 4-cyano-4-(phenylcarbonothioylthio)pentanoate (ANCP) was synthesized (Scheme 1a). Besides photo-cleavage and polymerizability, the presence of dithiobenzoate and hydroxyl functionalities in ANCP enables reversible addition-fragmentation chain transfer (RAFT) polymerization[71] and ring-opening polymerization (ROP). RAFT self-condensing vinyl copolymerization (RAFT SCVP) between ANCP and poly(ethylene glycol) methyl ether acrylate (PEGA) afforded hyperbranched poly(ANCP-*co*-PEGA) (PAP), and the hydroxyl moieties locating in each branching point were further used to initiate ROP of ε-caprolactone (CL) to generate PAP-*g*-PCL (HG1-HG3, Scheme 1b). On this basis, photo-triggered degradation and topological transition of PAP and HG3 were investigated, and a hydrophobic dye Nile red (NR) was encapsulated into HG3 aggregates to mimic photo-triggered release of hydrophobic drug. Our study affords an efficient approach to synthesis of novel stimuli-cleavable DHGCs via two step polymerizations, and the success of this research further paves way for exploring functional HGCs towards degradable structural transformation and potential applications in biomedical, surface and interface materials.

Experimental section

Materials

All the chemicals were purchased from Sigma-Aldrich unless otherwise stated. Poly(ethylene glycol) methyl ether acrylate (PEGA, $M_n \approx 480$, 99%) was passed through a basic alumina column to remove the inhibitor before use. ε-Caprolactone (CL, 99%) was distilled from calcium hydride under reduced pressure. Dichloromethane (DCM) were dried and distilled over CaH_2, dioxane and toluene were distilled over sodium and benzophenone, and 2,2′-azobis(isobutyronitrile) (AIBN) was recrystallized twice from ethanol. 4-Dimethylamino pyridine (DMAP) and *N*,*N*′-dicyclohexylcarbodiimide (DCC) were purchased from Sinopharm Chemical Reagent Co., Ltd. and used as received. Stannous octoate ($Sn(Oct)_2$, 97%), 2,2-bis(hydroxylmethyl)propionic acid (Bis-HMPA, 98%), 2,2′-dimethoxypropane (98%), sodium azide (99%, Alfa Aesar). 4-Cyanopentanoic acid dithiobenzoate (4-CPDB),[72] isopropylidene-2,2'-bis(methoxyl)propionic acid,[73] and 2-nitro-1,3-benzenedimethanol (NBD)[74] were synthesized and purified according to literature procedures.

Synthesis of HNCP

To a round flask were added 2-nitro-1,3-benzenedimethanol (NBD) (2.75g, 15.0 mmol), DCC (3.50 g, 17.0 mmol), DMAP (0.20 g, 1.64 mmol), and 100 mL of DCM under nitrogen, and the mixture was cooled with an ice−water bath. After stirring for 20 min, 25 mL of DCM solution containing 4-CPDB (2.79 g, 10.0 mmol) was added dropwise to the mixture in 1 h, and the reaction was further performed at 25 °C for 20 h. After filtration, the solution was washed with deionized water (30 mL × 3) and dried over $MgSO_4$. The crude product was purified by flash column chromatography eluting with mixture of ethyl acetate and petroleum ether (1:2, v/v), and 2.31 g (52% yield) of 3-hydroxymethyl-2-nitrobenzyl 4-cyano-4-(phenylcarbonothioyl thio)pentanoate (HNCP) was obtained as a red oil. ^{1}H NMR ($CDCl_3$): δ 7.91 (d, *J* 8.4, 2H, Ph*H*), 7.3-7.7 (m, 6H, Ph*H* and Ar*H*), 5.25 (s, 2H, ArCH_2O), 4.72 (s, 2H, CH_2OH), 2.3-2.8 (m, 4H, CH_2CH_2COO), 1.92 (s, 3H, CH_3). ^{13}C NMR ($CDCl_3$): δ 222.18 (*C*=S), 170.81 (*C*=O), 148.14, 144.22, 134.32, 133.04, 131.38, 129.47, 129.23, 128.48, 128.39, 126.54 (Ar*C* and Ph*C*), 118.36 (*C*N), 62.75, 60.82 (CH_2O), 45.51, 32.93, 29.41, 23.90. FT-IR (KBr): 3460, 3090, 3058, 2929, 1742, 1629, 1607, 1589, 1530, 1445, 1363, 1293, 1235, 1177, 1109, 1079, 1046, 998, 981, 868, 794, 763, 715, 687 cm^{-1}.

Synthesis of DNCP

HNCP (1.78 g, 4.0 mmol), isopropylidene-2,2-bis(methoxyl)propionic acid (7.0 g, 4.0 mmol), DMAP (0.073 g, 0.60 mmol) and 80 mL of DCM were added to a round flask under nitrogen, and the contents were cooled down and followed by slow addition of a 20 mL of DCM solution with DCC (0.83 g, 4.0 mmol) in 30 min. The mixture was further stirred at room temperature for 18 h. After filtration, the resultant mixture was concentrated and dissolved in 50 mL of THF. To the solution was added 20 mL of 1 M HCl, and the contents were stirred at room temperature for 18 h. After concentration under reduced pressure, the mixture was partitioned between water (50 mL) and DCM (150 mL), and the organic phase was repeatedly washed with deionized water until pH was close to 7. The organic solution was collected and dried with $MgSO_4$. The crude product was purified by flash column chromatography eluting with mixture of ethyl acetate and petroleum ether (1:1, v/v), and 1.79 g (80% yield) of 3-((2,2-dihydroxymethyl)propionyloxy)methyl-2-nitrobenzyl 4-cyano-4-(phenylcarbonothioylthio)pentanoate (DNCP) was isolated. ^{1}H NMR ($CDCl_3$): δ 7.91 (d, *J* 8.4, 2H, Ph*H*), 7.3-7.7 (m, 6H, Ph*H* and Ar*H*), 5.30 (s, 2H, ArCH_2O), 5.26 (s, 2H, ArCH_2O), 3.89, 3.74 (dd, *J* 11.2, 4H, CH_2OH), 2.2-2.8 (m, 4H, CH_2CH_2COO), 1.93 (s, CH_3), 1.07 (s, CH_3). ^{13}C NMR ($CDCl_3$): δ222.11 (*C*=S), 174.69, 170.62 (*C*=O), 148.29, 144.10, 132.91, 131.27, 129.96, 129.16, 128.74, 128.35, 126.40 (Ar*C* and Ph*C*),

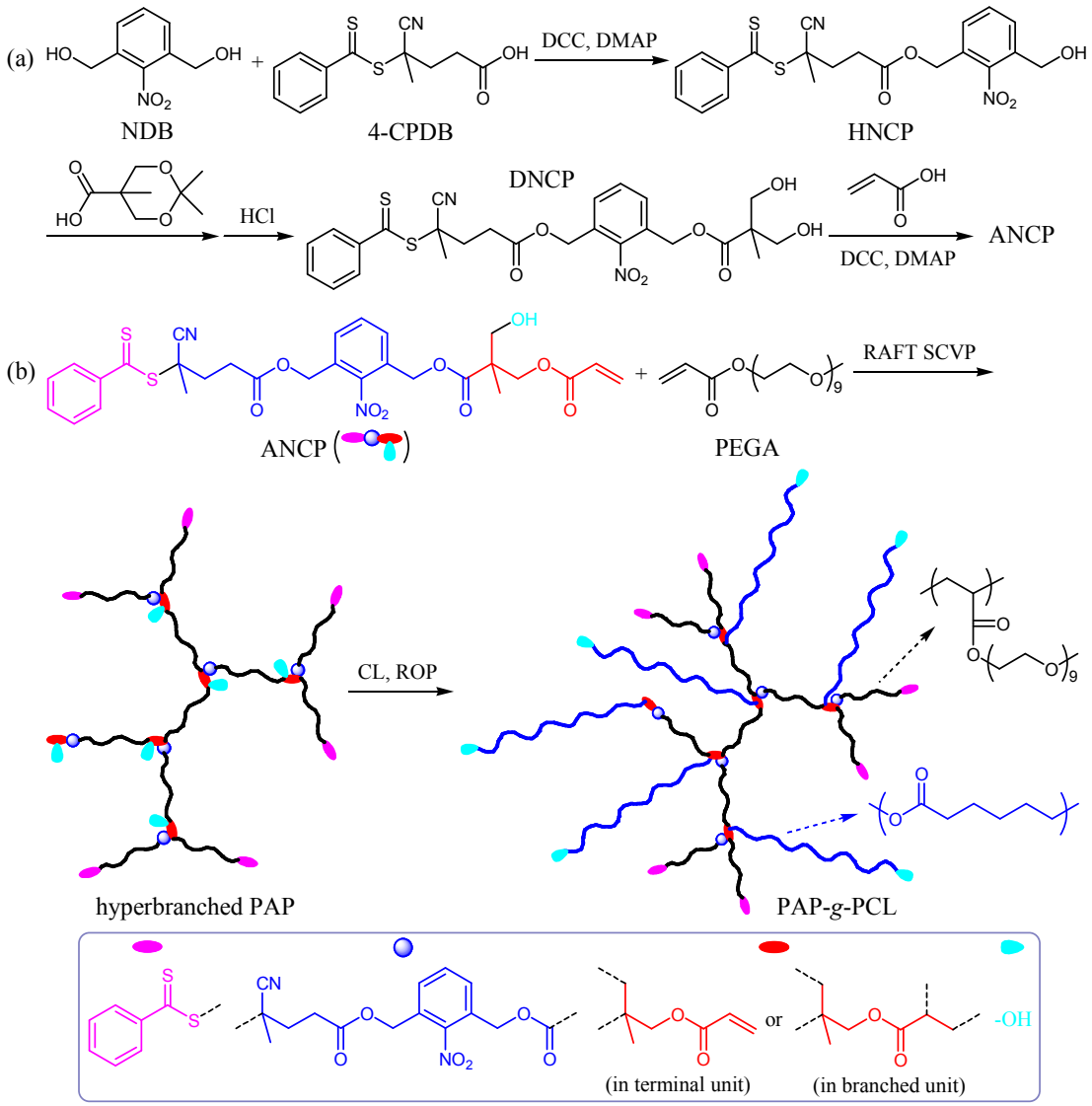

Scheme 1 Synthetic routes to photocleavable hyperbranched copolymer (poly(ANCP-*co*-PEGA), PAP) and hyperbranched graft copolymers (PAP-*g*-PCL, HG1-HG3) by successive RAFT SCVP and ROP using a multifunctional agent ANCP.

118.21 (*C*N), 66.13 (*C*H_2OH), 62.44, 62.30 (*C*H_2O), 49.48, 45.41, 32.77, 29.24, 23.73, 16.77. FT-IR (KBr): 3413, 3328, 3060, 2930, 2851, 1738, 1628, 1578, 1533, 1459, 1447, 1365, 1311, 1295, 1227, 1179, 1083, 1046, 999, 978, 903, 869, 854, 792, 764, 713, 688 cm^{-1}.

Synthesis of ANCP

To a round flask were added DNCP (1.01 g, 1.80 mmol), DCC (0.45 g, 2.18 mmol), DMAP (25 mg, 0.20 mmol), and 50 mL of DCM under nitrogen, and the contents were cooled down and followed by slow addition of a 10 mL of DCM solution comprising acrylic acid (0.13 g, 1.8 mmol) in 20 min. The mixture was further reacted at ambient temperature for 20 h. The crude product was filtered, concentrated and purified by flash column chromatography eluting with mixture of ethyl acetate and petroleum ether (1:1, v/v), and 0.72 g (65% yield) of 3-((2-acryloyloxymethyl-2-hydroxymethyl)propionyloxy)methyl-2-nitrobenzyl 4-cyano-4-(phenylcarbonothioylthio)pentanoate (ANCP) was obtained. ^{1}H NMR ($CDCl_3$): δ 7.91 (d, *J* 7.6, 2 H, Ph*H*), 7.3-7.7 (m, 6H, Ph*H* and Ar*H*), 6.40 (d, *J* 12.9, 1H, CH=CH_2), 6.10 (m, 1H, C*H*=CH_2), 5.84 (d, *J* 10.4, 1H, CH=CH_2), 5.27 (d, *J* 6.8, 4H, ArCH_2O), 4.39, 4.31 (dd, *J* 11.2, 2H, CH_2O), 3.68 (s, CH_2OH, 2H), 2.3-2.8 (m, 4H, CH_2CH_2C(=O)O), 1.93 (s, 3H, CH_3), 1.23 (s, 3H, CH_3). ^{13}C NMR ($CDCl_3$): δ 222.22 (*C*=S), 173.56, 170.79, 166.09 (*C*=O), 148.75, 144.41, 133.08, 131.67, 131.38, 130.34, 129.08, 128.57, 127.71, 126.64 (Ar*C*, Ph*C* and *C*H_2=CH_2), 118.40 (*C*N), 65.58 (*C*H_2O), 64.70 (*C*H_2OH), 62.78, 62.65 (Ar*C*H_2O), 48.61 (*C*CH$_2$OH), 45.61 (CH$_3$*C*CN), 33.09, 29.51 (*C*H_2), 24.08, 17.30 (*C*H_3). FT-IR (KBr): 3451, 3327, 3059, 3034, 2930, 2851, 1740, 1627, 1578, 1533, 1459, 1447, 1409, 1365, 1296, 1242, 1183, 1048, 984, 903, 869, 853, 808, 794, 765, 713, 689 cm^{-1}. Anal. Calcd for $C_{29}H_{30}N_2O_9S_2$: C, 56.66%; H, 4.92%; N, 4.56%; S, 10.43%. Found: C, 56.78%; H, 4.95%; N, 4.54%; S, 10.36%. MALDI-TOF MS: *m*/*z* = 637.136 $[M + Na]^+$ (theoretical value: 637.129), 653.107 $[M + K]^+$ (theoretical value: 653.103).

Synthesis of hyperbranched PAP by RAFT SCVP

To a Schlenk tube were added ANCP (184 mg, 0.3 mmol), PEGA (1.44 g, 3.0 mmol) and AIBN (4.9 mg, 0.03 mmol), and dioxane was added until the total volume was 3.0 mL. The contents were degassed with bubbled nitrogen for 20 min, and then the polymerization was performed at 65 °C for 18 h. The polymerization solution was precipitated into diethyl ether thrice, and 1.22 g (75.1% total monomer conversion) of poly(ANCP-*co*-PEGA) (PAP) was obtained after vacuum drying. PAP: ^{1}H NMR ($CDCl_3$): δ 7.95, 7.56, 7.52, 7.40 (m, Ph*H* and Ar*H*), 5.8-6.5 (m, residual C*H*=CH_2), 5.27 (d, *J* 10.0, ArCH_2O), 3.9-4.5 (m, CH_2OCO), 3.65 (s, CH_2CH_2O and CH_2OH), 3.38 (s, CH_3O), 0.7-2.8 (m, CH_2 and CH_3 originating from ANCP, and CH_2C*H* of PEGA unit). FT-IR (KBr): 3435, 2879, 1734, 1630, 1536, 1456, 1385, 1354, 1297, 1250, 1107, 951, 852, 813, 768, 688 cm^{-1}.

Synthesis of hyperbranched graft copolymers by ROP

In a typical experiment (run 4 of Table 1), PAP (0.208 g, 0.05 mmol OH), CL (0.570 g, 5.0 mmol), and Sn(Oct)$_2$ (4.1 mg, 0.01 mmol) were added to a Schlenk tube under nitrogen, and anisole was added until the total volume was 2.5 mL. The tube was degassed by three freeze−pump−thaw cycles and then placed in an oil bath thermostated at 120 °C for 20 h. The reaction mixture was precipitated in a large amount of hexane. After vacuum drying, 0.751 g (95.3% conversion) of PAP-*g*-PCL (HG3) was obtained. GPC-MALLS: M_n = 93600, PDI = 1.25. HG1 and HG2 were synthesized according to similar procedures. PAP-*g*-PCL: ^{1}H NMR ($CDCl_3$): δ 7.3-8.0 (m, Ph*H* and Ar*H*), 5.8-6.5 (m, residual C*H*=CH_2), 5.21 (s, ArCH_2O), 3.9-4.5 (m, CH_2OCO), 3.65 (s, CH_2CH_2O), 3.38 (s, CH_3O), 0.7-2.8 (m, CH_2 and CH_3 originating from ANCP, CH_2C*H* of PEGA, and CH_2CH_2CH_2CH_2COO of PCL). FT-IR (KBr): 3437, 2945, 2866, 1725, 1642, 1537, 1471, 1419, 1398, 1370, 1296, 1245, 1194, 1105, 1046, 962, 933, 842, 812, 797, 777, 732, 708, 693 cm^{-1}.

Photocleavable behaviors of PAP and HG3 aggregates

PAP solution in THF (c = 0.50 mg mL^{-1}) was exposed to UV irradiation (365 nm, 10.0 mW cm^{-2}) at 37 °C for different times. At a fixed time, the solution was drawn and subjected to UV-vis and GPC analyses. Similarly, HG3 aggregates (c = 0.50 mg mL^{-1}) in PBS solution (50 mM, pH 7.4) were subjected to UV irradiation (365 nm, 10.0 mW cm^{-2}) at 37 °C for a fixed time, and then the aggregation solution was isolated by lyophilization and subjected to GPC-MALLS analysis.

Formation of copolymer aggregates

HG3 (5.0 mg) was dissolved in 3.0 mL of THF and stirred for 1 h at room temperature. Then, the polymer solution was added dropwise into 7.0 mL of PBS solution (50 mM, pH 7.4) under vigorous stirring. Two hours later, the solution was transferred into dialysis membrane tubing (MWCO 10 kDa) and dialyzed against PBS solution (50 mM, pH 7.4) for 24 h to remove the organic solvent. The micellar solution was stored at 4 °C before measurements, and the diameter and morphology of aggregates were determined by DLS and TEM, respectively.

***In vitro* Nile red release from HG3 aggregates**

HG3 (15.0 mg) and Nile red (3.0 mg) were dissolved in THF (30 mL), and followed by slow addition of 90 mL of PBS solution (10 mM, pH 7.4) to induce the formation of NR-loaded polymeric micelles. After 3-h vigorous stirring, 80 mL of PBS solution was added to precipitate unencapsulated dye, and the solution obtained was filtered through Millipore membrane with 0.45 μm pore size. THF and most of water were removed at 30 °C under reduced pressure, and the solution was further dialyzed against PBS solution (50 mM, pH 7.4) for 12 h to afford copolymer aggregates ($c_{polymer}$ = 0.45 mg mL^{-1}). The drug loading capacity (DLC = 6.92%) and drug loading efficiency (DLE = 34.6%) of NR-loaded aggregates were determined by fluorescence analysis. On this basis, the copolymer aggregates were subjected to NR release with or without UV irradiation (365 nm, 10.0 mW cm^{-2}) at 37 °C. At predetermined time intervals, part of solution was drawn to measure the fluorescence spectroscopy, and the release profiles were obtained. All release experiments were performed in triplicate. Photobleaching of Nile red in saturated aqueous solution and PEG-*b*-PCL aggregates was performed according to similar procedures.

Characterization

The apparent number-average molecular weight ($M_{n,GPC}$) and polydispersity (PDI) of linear polymer, hyperbranched PAP and its photocleavable samples were measured on a TOSOH HLC-8320 gel permeation chromatography (GPC) using three TSKgel SuperMultipore HZ-M columns at 40 °C. THF was used as an eluent at a flow rate of 0.35 mL min^{-1}, and the samples were calibrated with PMMA standard samples. Gel permeation chromatography with multiple angle laser scattering detection (GPC-MALLS) system was used to determine the absolute number-average molecular weight ($M_{n,LS}$) and polydispersity of hyperbranched and hyperbranched graft polymers. GPC was conducted in THF at 35 °C with a flow rate of 1.0 mL min^{-1}, and three TSK-GEL H-type columns with 5 μm bead size were used. Data were collected and processed by use of ASTRA software from Wyatt Technology, and molecular weights were determined by the triple detection method. ^{1}H (400 MHz) and ^{13}C (100 MHz) NMR spectra were recorded on a Varian spectrometer at 25 °C in $CDCl_3$. C, H, N and S were determined by combustion followed by chromatographic separation and thermal conductivity detection using a Carlo-Erba EA 1110CHNO-S Elemental Analyzer. Matrix assisted laser desorption/ionization time of flight (MALDI-TOF) mass spectrum was measured on a Bruker UltrafleXtreme mass spectrometer equipped with a 1 kHz smart beam-II laser. Fourier Transform Infrared (FT-IR) spectra were recorded on a Perkin-Elmer 2000 spectrometer using KBr discs. UV irradiation (365 nm, 10.0 mW cm^{-2}) of PAP solution and HG3 aggregates was performed using a Shimadzu UV-2600 spectrophotometer at 37 °C. UV-vis absorption spectra were recorded on a Shimadzu UV-3150 spectrophotometer, and fluorescence spectra were recorded at 25 °C on a FLS920 fluorescence spectrometer with an excitation wavelength of 560 nm. Dynamic light scattering (DLS) measurements were conducted at 25 °C using Zetasizer Nano-ZS from Malvern Instruments equipped with a 633 nm He–Ne laser using back-scattering detection. Transmission electron microscopy (TEM) images were obtained through a Hitachi H-600 electron microscope.

Table 1 Results for synthesis of hyperbranched PAP (run 1, DB = 0.20) and PAP-*g*-PCL copolymers (runs 2-4)[a]

run	polymer	CTA/MI[b]	M	DP_0	solvent	T (°C)	t (h)	C%[c]	$M_{n,th}$[d]	M_n[e]	PDI[e]	$M_{n,NMR}$[f]
1	PAP	ANCP	PEGA	10	toluene	65	18	75.1	—	25400	1.35	—
2	HG1	PPEGA	CL	30	anisole	120	20	90.8	44300	45500	1.21	44600
3	HG2	PPEGA	CL	60	anisole	120	20	95.6	65300	65300	1.24	67700
4	HG3	PPEGA	CL	100	anisole	120	20	95.3	91700	93600	1.25	93500

[a] Reaction conditions: $[PEGA]_0:[ANCP]_0:[AIBN]_0$ = 10:1:0.1, $[PEGA]_0$ = 1.0 mol L^{-1} (run 1); $[CL]_0:[OH]_0:[Sn(Oct)_2]_0 = DP_0$:1:0.2, $[CL]_0$ = 2.0 mol L^{-1} (runs 2-4). [b] Chain transfer agent (CTA) or macroinitoator (MI). [c] Monomer conversion determined by gravimetry. [d] Theoretical molecular weight, $M_{n,th} = M_n(PAP) + 6.1MW_{CL} \times DP_0 \times$ conversion. [e] Number-average molecular weight (M_n) and polydispersity (PDI) determined by GPC-MALLS. [f] Number-average molecular weight given by ^{1}H NMR analysis.

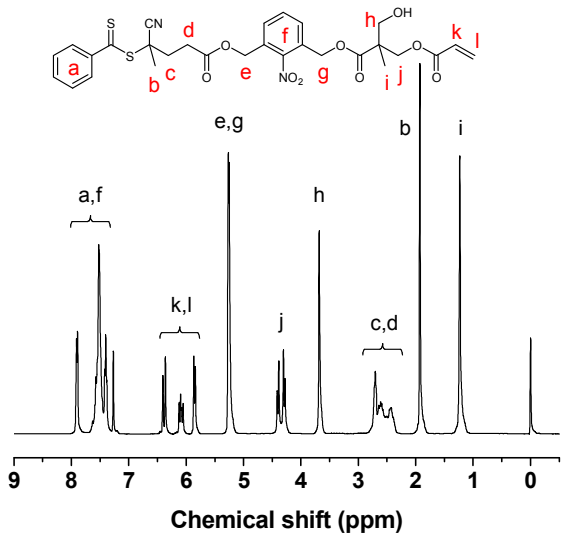

Fig. 1 ^{1}H NMR spectrum of ANCP.

Results and discussion

Synthesis of DHGCs

A multifunctional agent ANCP with ONBE, acrylate, hydroxyl and dithiobenzoate functionalities were synthesized, and then the target copolymers were synthesized by successive RAFT SCVP and ROP. The detailed syntheses were described blow.

First, ANCP was synthesized by four step reactions (Scheme 1a). Esterification between 2-nitro-1,3-benzenedimethanol (NBD)[74] and 4-cyanopentanoic acid dithiobenzoate (4-CPDB) afforded 3-hydroxymethyl-2-nitrobenzyl 4-cyano-4-(phenylcarbonothioyl thio)pentanoate (HNCP, see Fig. S1 for ^{1}H and ^{13}C NMR spectra) in 52% yield. A second esterification between HNCP and isopropylidene-2,2-bis(methoxyl)propionic acid was performed, and the crude product was subjected to deprotection using 1 M HCl in THF. After purification by flash column chromatography eluting with ethyl acetate / petroleum ether (1:1, v/v), 3-((2,2-dihydroxymethyl)propionyloxy)methyl-2-nitrobenzyl 4-cyano-4-(phenylcarbonothioylthio)pentanoate (DNCP, see Fig. S2 for ^{1}H and ^{13}C NMR spectra) was isolated in 80% yield. On this basis, a third esterification between DNCP and acrylic acid was conducted to afford ANCP in 65% yield. In ^{1}H NMR spectrum of ANCP (Fig. 1), characteristic signals were noted at 7.91 (2 H of Ph*H* in dithiobenzoate), 6.40, 5.84 (CH=CH_2), 6.10 (C*H*=CH_2), 5.27 (ArCH_2O), 4.39, 4.31 (CH_2O), 3.68 (CH_2OH), 1.93 and 1.23 ppm (CH_3), and typical signals appeared at 222.22 (*C*=S), 173.56, 170.79, 166.09 (*C*=O), 148.75, 144.41, 133.08, 131.67, 131.38, 130.34, 129.08, 128.57, 127.71, 126.64 (Ar*C*, Ph*C* and CH_2=*C*H_2), 118.40 (*C*N), 65.58 (*C*H_2O), 64.70 (*C*H_2OH), 62.78, 62.65 (ArCH_2O), 24.08 and 17.30 ppm (*C*H_3) in ^{13}C NMR spectrum (Fig. S3).

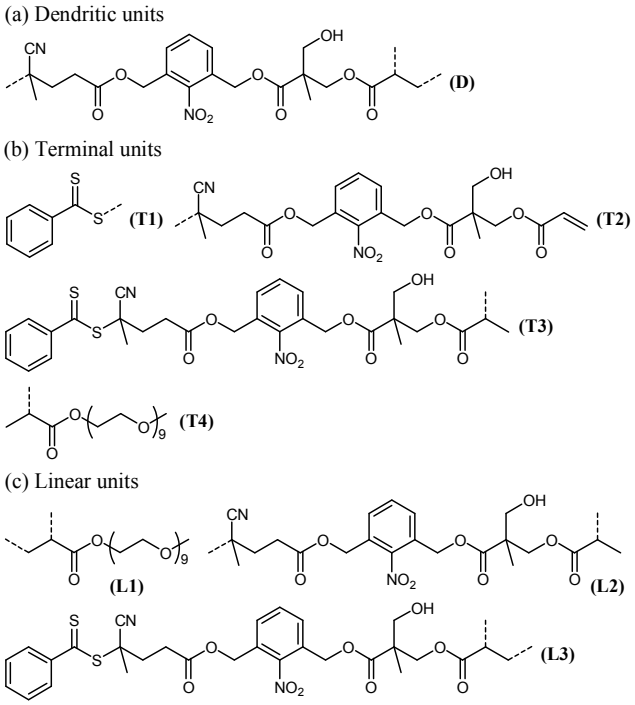

Scheme 2 Possible structural units of hyperbranched PAP.

Second, RAFT copolymerization of ANCP and PEGA via self-condensing vinyl copolymerization was performed to generate functional hyperbranched PAP. In addition to reactive dithiobenzoate moieties in the chain end of each branch, PAP had both ONBE and hydroxyl functionalities in each branching point, which allowed photo-triggered degradation as well as versatile postmodification reactions. As RAFT SCVP ($[PEGA]_0:[ANCP]_0:[AIBN]_0$ = 10:1:0.1, $[PEGA]_0$ = 1.0 mol L^{-1}) was conducted in toluene at 65 °C for 18 h, PAP was obtained in a total conversion

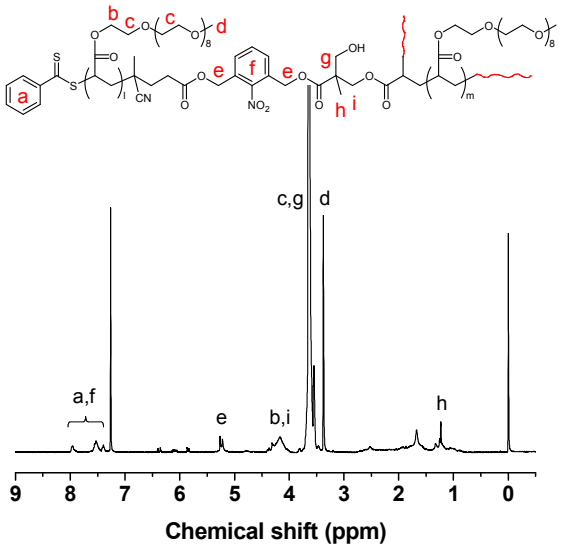

Fig. 2 ^{1}H NMR spectrum of hyperbranched PAP (the wavy line denotes PPEGA branches and branched building blocks originating from ANCP).

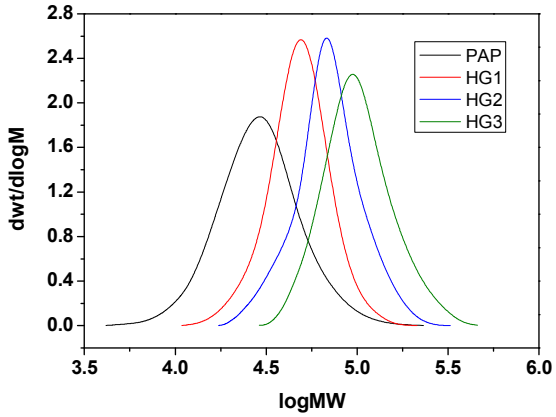

Fig. 3 GPC traces of hyperbranched PAP and PPEGA-*g*-PCL (HG1-HG3).

of 75.1% (run 1 of Table 1). In ^{1}H NMR spectrum (Fig. 2), characteristic signals originating from ANCP were observed at 7.95, 7.56, 7.52, 7.40 (Ph*H* and Ar*H*), 5.8-6.5 (residual C*H*=CH_2), 5.27 (ArCH_2O) and 1.23 ppm (CH_3), and other signals resulting from PPEGA branches were primarily noted at 4.17 (COOCH_2), 3.65 (CH_2CH_2O, overlapped with CH_2OH), 3.38 (terminal CH_3O), 2.53 (CH$_2$C*H* of PEGA unit, overlapped with CH_2 originating from ANCP), and 0.7-2.0 ppm (CH_2CH of PEGA unit, overlapped with CH_3 originating from ANCP). The feed ratio of [PPEGA]$_0$:[ANCP]$_0$ ($F = 2I_{3.38}/(3I_{7.95})$) was calculated as 7.4 by comparing the integrated signal areas in ^{1}H NMR spectroscopy. By assuming ANCP had quantitatively participated in the SCVP process, the feed ratio of [PPEGA]$_0$:[ANCP]$_0$ in PAP was deduced as 7.2 based on the total conversion. Both of them were similar, revealing lack of significant loss of chain transfer agent (CTA) functionality during copolymerization. To calculate the degree of branching (DB), all the possible structural units of PAP are listed in Scheme 2. Taking account of the high reactivity of acrylates during RAFT process mediated by dithiobenzoate, structural units T3, T4 and L2 formed by termination of chain radical to capture one proton could be neglected. Characteristic signals of various structural units appeared at 5.1-5.4 (ArCH_2O of D, T2 and L3), 7.95 (2H of Ph*H*, T1), 5.8-6.5 (CH_2=C*H* of T2), 2.3-2.8 (CH_2CH_2COO of L3, which was overlapped with C*H*COO of PEGA unit), and 3.38 ppm (CH_3O of L1). Based on the equation DB = $(D + T)/(D + T + L) = (12I_{7.95} + I_{3.38} - 3I_{2.0\text{-}2.8})/(12I_{7.95} + 5I_{3.38} - 3I_{2.0\text{-}2.8})$ (where D, T, and L represent the fractions of the branched, terminal, and linear units, respectively), the degree of branching of PAP was deduced to be about 0.20 by assuming no CTA functionality was lost. ^{1}H NMR analysis confirmed the formation of branched structure in PAP obtained by RAFT SCVP. Based on GPC-MALLS analysis, PAP had number-average molecular weight ($M_{n,LS}$) of 25400 and polydispersity (PDI) of 1.35, and its GPC trace only exhibited monomodal distribution (Fig. 3). Therefore, the number-average functionality (f) of ONBE, dithiobenzoate, and hydroxyl moieties in each PAP was about 6.1.

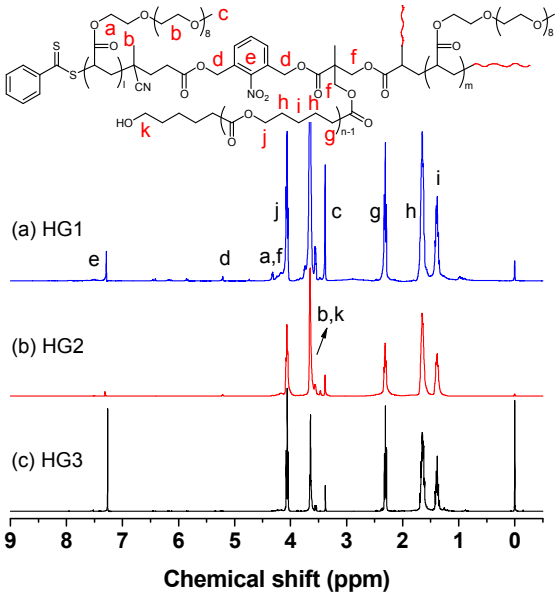

Fig. 4 ^{1}H NMR spectra of DHGCs (the wavy line denotes PPEGA branches, branched building blocks originating from ANCP, and PCL grafts).

Last, hydroxyl-functionalized PAP was used as macroinitiator to initiate CL polymerization to synthesize DHGCs. As CL polymerizations using Sn(Oct)$_2$ catalyst and different feed ratios ([CL]$_0$:[OH]$_0$ = 30, 60 and 100) were performed in anisole at 120 °C for 20 h, three PAP-*g*-PCL copolymers (HG1-HG3) were obtained. Besides typical signals originating from PPEGA branches and dendritic units, new signals corresponding to PCL grafts appeared at 4.06 (CH_2O), 2.31 (CH_2CO), 1.65 (CH_2CH$_2$CH_2CH$_2$COO), and 1.38 ppm (CH$_2$CH_2CH$_2$CH$_2$COO) in ^{1}H NMR spectra (Fig. 4). Based on the equation $DP_{PCL} = 3I_{2.31} \times m_{PEGA}/(2I_{3.38} \times m_{ANCP})$ (m_{PEGA}/m_{ANCP} mean the feed ratio of

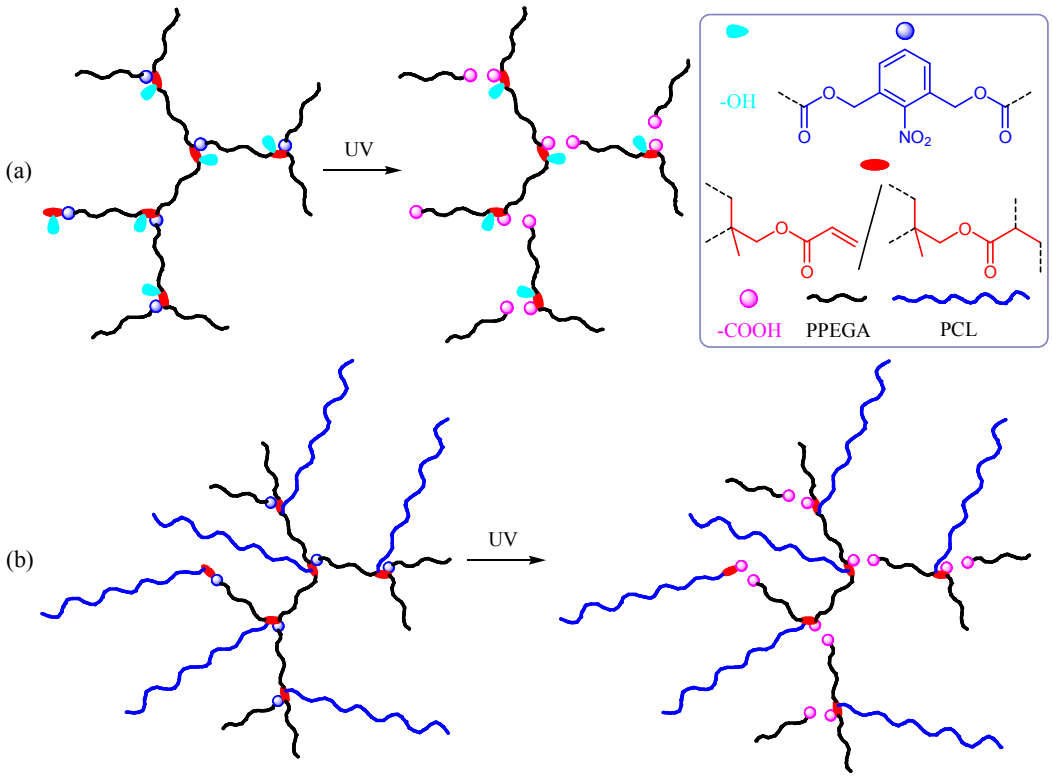

Scheme 3 Light-triggered degradation and topological transformation of hyperbranched PAP (a, from hyperbranched copolymer to linear homopolymer and random copolymer) and PAP-*g*-PCL (b, from hyperbranched graft copolymer to linear, star and graft polymers).

PEGA to ANCP units), the polymerization degree of PCL grafts were calculated as 27.6 (HG1), 60.8 (HG2) and 98.0 (HG3), and $M_{n,NMR}$ values were determined to be within 44600-93500 using the equation $M_{n,NMR} = M_{n,LS}(PAP) + 6.1MW_{CL} \times DP_{PCL}$. GPC-MALLS analyses indicated the $M_{n,LS}$ values of HG1-HG3 ranged between 45500 and 93600, with polydispersity indices in the range 1.21-1.25 (Fig. 3). As compared with PAP, the GPC traces of HG1-HG3 gradually shifted to higher molecular weight sides, revealing the efficient chain extension polymerization. As listed in runs 2-4 of Table 1, the $M_{n,LS}$ and $M_{n,NMR}$ values were roughly comparable, and both were close to the theoretical molecular weights ($M_{n,th}$).

Last, hydroxyl-functionalized PAP was used as macroinitiator to initiate CL polymerization to synthesize DHGCs. As CL polymerizations using $Sn(Oct)_2$ catalyst and different feed ratios ($[CL]_0$:$[OH]_0$ = 30, 60 and 100) were performed in anisole at 120 °C for 20 h, three PAP-*g*-PCL copolymers (HG1-HG3) were obtained. Besides typical signals originating from PPEGA branches and dendritic units, new signals corresponding to PCL grafts appeared at 4.06 (CH_2O), 2.31 (CH_2CO), 1.65 ($CH_2CH_2CH_2CH_2COO$), and 1.38 ppm ($CH_2CH_2CH_2CH_2COO$) in ^{1}H NMR spectra (Fig. 4). Based on the equation $DP_{PCL} = 3I_{2.31} \times m_{PEGA}/(2I_{3.38} \times m_{ANCP})$ (m_{PEGA}/m_{ANCP} mean the feed ratio of PEGA to ANCP units), the polymerization degree of PCL grafts were calculated as 27.6 (HG1), 60.8 (HG2) and 98.0 (HG3), and $M_{n,NMR}$ values were determined to be within 44600-93500 using the equation $M_{n,NMR} = M_{n,LS}(PAP) + 6.1MW_{CL} \times DP_{PCL}$. GPC-MALLS analyses indicated the $M_{n,LS}$ values of HG1-HG3 ranged between 45500 and 93600, with polydispersity indices in the range 1.21-1.25 (Fig. 3). As compared with PAP, the GPC traces of HG1-HG3 gradually shifted to higher molecular weight sides, revealing the efficient chain extension polymerization. As listed in runs 2-4 of Table 1, the $M_{n,LS}$ and $M_{n,NMR}$ values were roughly comparable, and both were close to the theoretical molecular weights ($M_{n,th}$).

The afore-mentioned results indicated the target DHGCs could be efficiently synthesized by successive RAFT SCVP and ROP.

Photocleavable behaviors of PAP

The introduction of cleavable moieties in star,[38,76] branched[13,19,20,38] and graft[77,78] polymers usually allows stimuli-triggered degradation and topological transition. As well documented, ONBE linkages can be cleaved upon UV irradiation,[39–48] and thus versatile structural transformations are readily achieved in this study. In theory, hyperbranched PAP can be converted into linear polymers comprising PPEGA segments and carboxyl / hydroxyl functionalities as all the ONBE moieties are cleaved (Scheme 3a). To reveal the photocleavable ability of hyperbranched polymer, PAP solution in THF (c = 0.50 mg mL^{-1}) was subjected to UV irradiation (365 nm, 10.0 mW cm^{-2}) for different times, and the process was monitored by UV-vis spectroscopy and GPC analysis. With prolonging UV irradiation time, the absorption peak at 299 nm resulting from dithiobenzoate and ONBE functionalities was gradually weakened, and the maximum absorption slightly decreased from 299 to 294 nm (Fig. 5A), and the solution colour changed from red to yellowish. Meanwhile, the absorption at about 248 nm originating from *o*-nitrosobenzyl derivative was liable to increase with extended

time, and the maximum absorption slightly increased from 248 to 251 nm. As the irradiation time was beyond 10 min, the UV-vis spectrum only slightly changed, which was similar to the results noted in other *o*-nitrobenzyl-bearing polymers.[39–43,48] As estimated by conventional GPC using THF as an eluent, PAP had apparent molecular weight ($M_{n,GPC}$) of 17500 and polydispersity of 1.39 (a of Fig. 5B). Upon UV irradiation, the GPC traces of cleaved polymers gradually shifted to low-molecular-weight side, and a bimodal distribution appeared (b-e of Fig. 5B). As the irradiation time increased from 2 to 30 min, the $M_{n,GPC}$ values decreased from 6230 to 3690, and the polydispersity indices were about 1.4. The photocleaved samples obtained at 10 and 30-min irradiation had similar apparent molecular weights, which was in accordance with the result observed in UV-vis spectroscopy. These results confirmed the photo-triggered degradation of hyperbranched PAP.

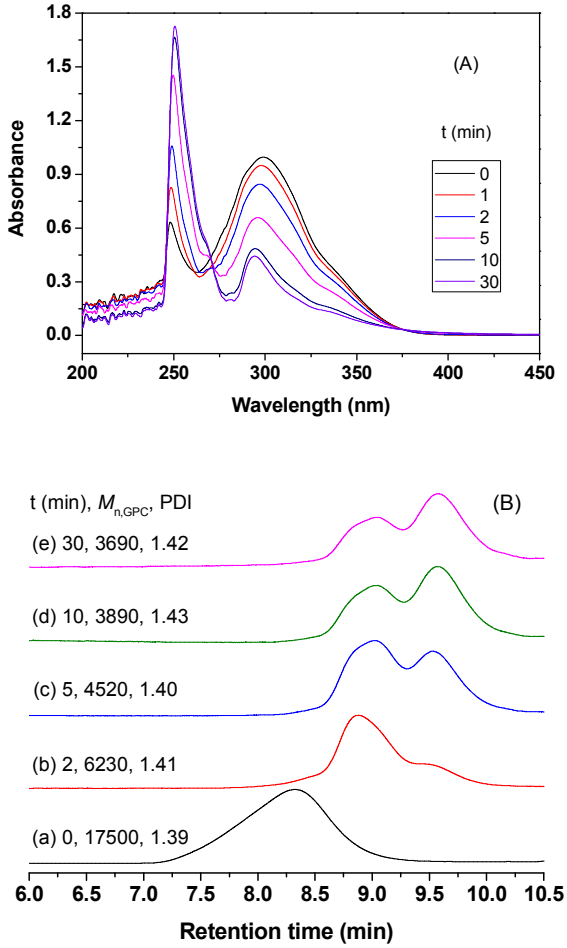

Fig. 5 (A) UV-vis absorption spectra recorded as a function of UV irradiation time; (B) GPC traces of original PAP (a) and its photocleaved samples (b-e), in which PAP solution in THF (c = 0.50 mg mL^{-1}) was subjected to UV irradiation (365 nm, 10.0 mW cm^{-2}) for different times.

Photo-triggered degradation and morphological transition of HG3 aggregates

With the complete cleavage of ONBE moieties, PAP-*g*-PCL can be potentially degraded into mixtures of linear, starlike and graft polymers (Scheme 3b). For the latter mixtures, linear polymer can be either PPEGA (originating from PPEGA branches) or PCL (resulting from CL polymerization initiated from hydroxyl functionality connecting with terminal acrylic unit), star polymer contains PPEGA and PCL arms, and graft copolymer comprises PPEGA backbone and PCL grafts. The photo-triggered degradation may have a great potential in inducing morphological transition and smart drug delivery system.

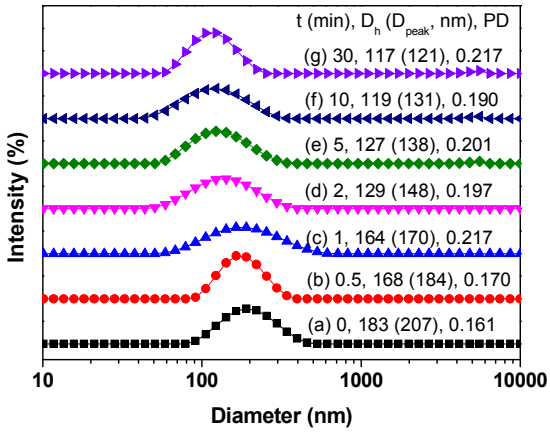

Fig. 6 DLS plots of copolymer aggregates (c = 0.50 mg mL^{-1}) formed from HG3 in PBS solution (50 mM, pH 7.4) before (a) and after (b-g) UV irradiation for different times.

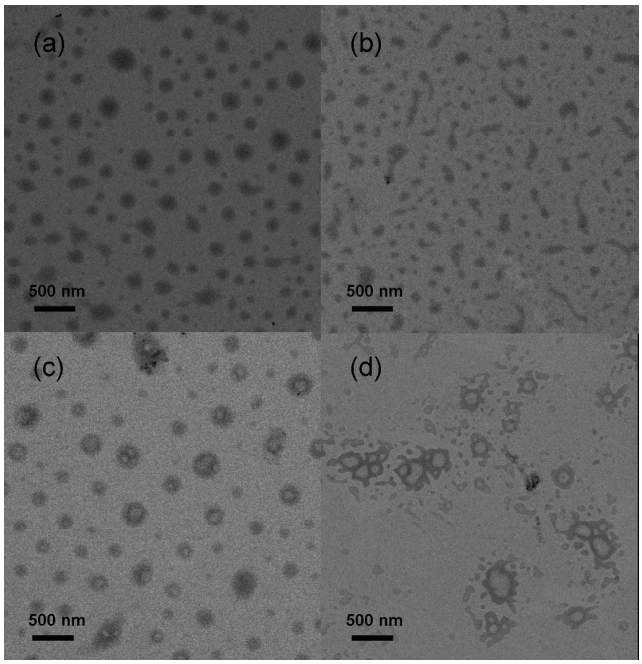

Fig. 7 TEM images of HG3 aggregates (c = 0.50 mg mL^{-1}) before (a) and after (b-d) UV irradiation for 1 min (b), 5 min (c) and 10 min (d).

To reveal the influence of UV irradiation on degradation and reaggregation behaviors of DHGCs, HG3 was chosen as a typical sample to perform aqueous self-assembly and followed by UV irradiation for different times. In the absence of light irradiation,

HG3 aggregates (c = 0.50 mg mL^{-1}) exhibited monomodal distribution in DLS plots (Fig. 6a), and the average hydrodynamic diameter (D_h), peak size (D_{peak}) and particle size distribution (PD) were 183 nm, 207 nm and 0.161, respectively. The sizes of HG3 aggregates given by DLS and TEM were roughly comparable, and TEM image indicated the aggregates were spherical micelles (Fig. 7a). As the copolymer micelles were exposed to UV irradiation (365 nm, 10.0 mW cm^{-2}) at 37 °C for a time period up to 30 min, the D_h values of the resultant copolymer aggregates gradually decreased from 168 nm (t = 0.5 min) to 117 nm (t = 30 min), and the PD values were in the range 0.170-0.217. TEM images confirmed the evolution in morphological transition upon UV irradiation. With increasing irradiation time, the morphologies of copolymer aggregates continuously varied from spherical micelles (t = 0) to mixtures of spherical and wormlike micelles (t = 1 min, Fig. 7b), mixtures of micelles and vesicles (t = 2 min), and vesicles containing multicompartment vesicles (t ≥ 5 min, c and d of Fig. 7). The photocleaved samples were isolated by lyophilization and subjected to GPC-MALLS analysis. As compared with HG3, the cleaved polymers exhibited broadened molecular weight distribution in GPC traces (PDI = 1.54-1.68, Fig. 8), and their molecular weights of various polymers were significantly decreased from 93600 (original one) to 26500 (1 min), 19000 (5 min) and 12200 (30 min). These results revealed that ONBE linkages in copolymer aggregates could be rapidly cleaved even if relatively short irradiation time was applied, resulting in low-molecular-weight polymers comprising PPEGA and PCL segments. Therefore, the remarkable morphological transition could be ascribed to photo-triggered degradation of HG3 copolymer and reassembly of cleaved polymers. The continuous changes in end group, molecular weight and topology strongly induced the dynamic change in mutual interactions among polymer segments, resulting in the formation of different nanoobjects involving multicompartment vesicles.

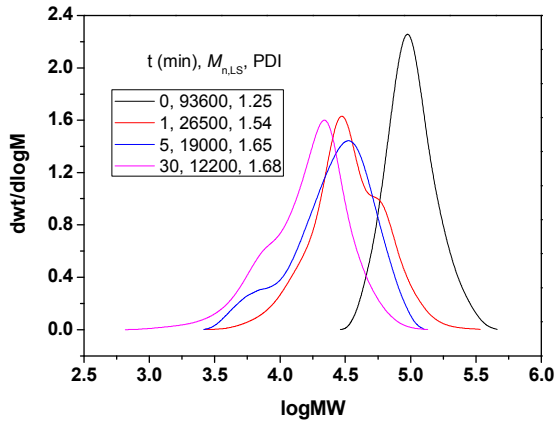

Fig. 8 GPC traces of HG3 and its photocleaved samples, in which the copolymer aggregates (c = 0.50 mg mL^{-1}) were subjected to UV irradiation for different times.

Photo-triggered *in vitro* release of Nile red from copolymer aggregates

Photo-cleavage of functional polymers has proven to hold great promise in smart drug delivery systems.[39–58] Upon UV irradiation, ONBE bearing DHGCs can be readily cleaved, leading to the formation of linear and branched copolymers. To reveal their potential in biomedical application, a hydrophobic dye Nile red was encapsulated into HG3 aggregates to mimic the release process of hydrophobic drug, and the influence of UV irradiation on release properties were investigated. As compared with blank HG3 micelles, the hydrodynamic diameter of NR-loaded HG3 aggregates ($c_{polymer}$ = 0.45 mg mL^{-1}) formed in PBS solution (50 mM, pH 7.4) at 37 °C was increased to 244 nm, and the particle size distribution was slightly reduced (PD = 0.144) in DLS plots (Fig. S6). As determined by fluorescence analysis, the drug loading capacity (DLC) and drug loading efficiency (DLE) of NR-loaded HG3 aggregates were 6.92% (for DLC) and 34.6% (for DLE), respectively. On this basis, the photo-triggered release properties of NR-loaded aggregates with or without UV irradiation were investigated. Since the fluorescence emission of Nile red is very small in water due to low solubility and extremely intense as solubilized in the hydrophobic micellar core, the release process can be directly monitored via measuring the change in fluorescence spectroscopy of Nile red.[54,75]

To reveal the photobleaching degree of the dye, both saturated aqueous solution of Nile red and NR-loaded PEG-*b*-PCL aggregates lacking stimuli-responsiveness were initially subjected to UV irradiation. Based on the normalized fluorescence intensity (NFI), about 1.04% of Nile red remained in the saturated aqueous solution and about 99% of NR was encapsulated in HG3 aggregates at the beginning of release (t = 0). As the saturated aqueous solution of NR prepared by dialysis was exposed to UV light for 30 min, the NFI value was only slightly decreased (NFI(30)/NFI(0) = 0.950, Fig. S7), suggesting the photobleaching of NR saturated solution during release was not significant. Since the concentration of NR was very low, the influence of photobleaching of NR saturated solution on release was quite limited. Meanwhile, PEG_{45}-*b*-PCL_{42} (in which the subscript denotes the degree of polymerization, $M_{n,NMR}$ = 6800, PDI = 1.18, Fig. S8) was synthesized to investigate the photobleaching effect of encapsulated NR. As the copolymer aggregates (DLC = 8.24%) were treated with UV irradiation for 1-30 min, the NFI value was gradually decreased from 1.0 to 0.946, and the differences in NFI values obtained with or without UV irradiation for different times were within ±0.0026 (Fig. S9 and Fig. S10). Taking account of the experimental errors (within ±0.005 for triplicate experiments), two release curves were quite similar, revealing the photobleaching of encapsulated NR was also limited. These results indicated the photobleaching effect of Nile red in aqueous solution and copolymer aggregates was almost negligible as they were subjected to UV irradiation for a time period up to 30 min.

Meanwhile, the influence of irradiation time on release properties was investigated. To this end, NR-loaded aggregates were exposed to UV irradiation for 0.5-30 min, and the fluorescence spectra were monitored. With prolonging irradiation time, the maximum fluorescence intensity was liable to decrease (Fig. 9a), and the NFI value in Fig. 9b was gradually reduced to 0.946 (0.5 min), 0.911 (1 min), 0.825 (2 min), 0.719 (5 min), 0.624 (10 min) and 0.524 (30 min). These results revealed the

release process could be efficiently adjusted by control over irradiation time. Considering the negligible contribution of released dye on fluorescence intensity, it was deduced about 47.6% of the encapsulated dye could be released from the copolymer aggregates as 30-min UV irradiation was applied. This phenomenon could be attributed to photo-triggered destabilization and reassembly of copolymer aggregates, during the dynamic process the loaded dye molecules were fast released.

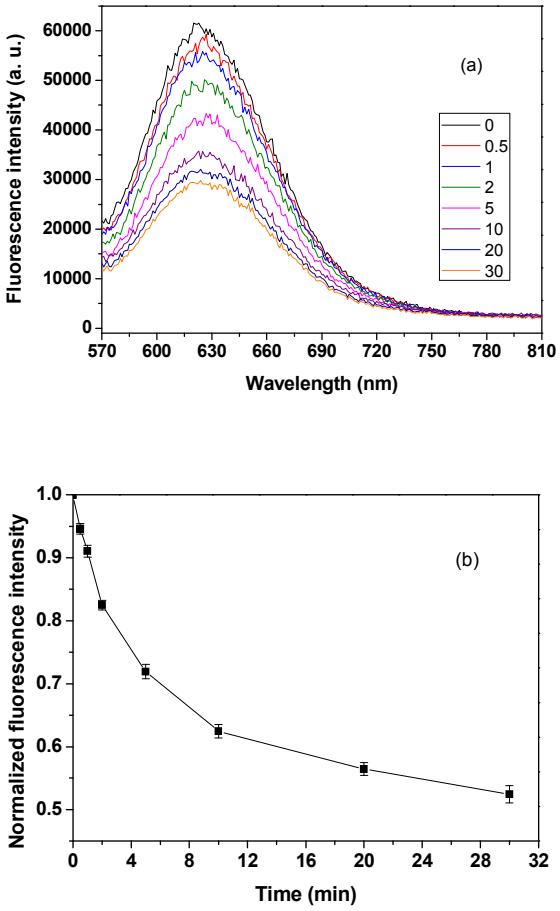

Fig. 9 Influence of UV irradiation time (min) on fluorescence spectra (a, λ_{ex} = 550 nm) and normalized fluorescence intensity (b) of NR-loaded HG3 aggregates ($c_{polymer}$ = 0.45 mg mL^{-1}) in PBS solution (50 mM, pH 7.4) at 37 °C.

On this basis, the release properties with or without light irradiation were further investigated. Considering 1-min UV irradiation could lead to the instantaneous release of about 8.9% of encapsulated NR from copolymer aggregates, 1 min was chosen as the photo-stimulus time, and UV irradiation was performed via either normal or "on-demand" mode (Fig. S11). For normal photo-triggered release, 1-min UV irradiation was conducted at the beginning of release process. For on-demand photo-triggered release, the same irradiation treatment (10.0 mW cm^{-2}, 60 s) was repeatedly applied at 0, 30, 60, 120 and 180 min, respectively. In the absence of UV irradiation, the NFI value was gradually decreased with extended time and dropped to about 0.688 at 12 h (Fig. 10a), corresponding to a relatively slow process with sustained release. With 1-min UV irradiation in the initial stage, the NFI value was immediately decreased from 1 (0 min) to 0.911 (1 min), and then slowly dropped to around 0.417 at 12 h (Fig. 10b). For releases with or without 1-min UV irradiation, the difference of NFI could reach up to 0.182 at 12 h, which was higher than that observed at the initial 1-min photo-stimulus (ΔNFI = 0.089). Careful inspection of Fig. 10 revealed the NFI differences of curves a and b at a fixed time were liable to increase with prolonging time and almost reach to a maximum at about 180 min. This phenomenon could be ascribed to the destabilization of copolymer aggregates, in which 1-min UV irradiation led to partial cleavage of ONBE linkages, and then the reaggregation of NR-loaded copolymer aggregates was dynamically performed until a thermodynamic equilibrium was reached. During the reassembly process, increasing encapsulated dye molecules could efficiently diffuse into aqueous solution, resulting in a relatively fast release after cutting off the UV irradiation. Given the effect of off-state drug leakage from copolymer aggregates, the "on-off" release mode[49,57] could not be rigorously performed during the release process from NR-loaded HG3 aggregates. Moreover, on-demand photo-stimulus could result in a fast release in a fixed time point, evident from the release profiles as listed in Fig. 10c. As 1-min UV irradiation was individually applied at a particular time (t_0), the NFI_{t0} - NFI_{t0+1} values were 1 - 0.911 (t_0 = 0), 0.798 - 0.724 (t_0 = 30 min), 0.694 - 0.633 (t_0 = 60 min), 0.562 - 0.507 (t_0 = 120 min) and 0.440 - 0.401 (t_0 = 180 min), and the NFI value was remarkably dropped to 0.235 at 12 h. These results revealed 1-min UV irradiation could result in an accelerative release, and the instantaneous release amount of Nile red was gradually dropped from 0.089 (t_0 = 0) to 0.039 (t_0 = 180 min). When copolymer aggregates were exposed to UV irradiation, the ONBE linkages were gradually cleaved, and the change in chemical composition, molecular weight and topology could induce the reassembly of copolymer aggregates since they were far from the thermodynamic equilibrium, during which part of loaded dye molecules were rapidly released. As the particular time for UV irradiation was extended, the remaining ONBE linkages were reduced, and the different degree in molecular parameters and macromolecular architecture before and after light irradiation was reduced. Consequently, the enhancement in instantaneous release induced by 1-min UV irradiation was continuously lowered due to the reduced change in microenvironment with time going on.

As compared with the release of Nile red lacking external stimulus, the release rate, instantaneous and cumulative releases from copolymer aggregates could be tuned in a wide range as UV-stimulus was applied, and the photo-triggered release process could be efficiently controlled by choosing different irradiation time and changing the photo-stimulus modes. By contrast to normal photo-induced release with a fixed irradiation time, the on-demand UV-triggered release is more promising due to the burst release upon exposure to UV irradiation and the faster release in the "light-off" state. Additionally, the release kinetics is potentially adjustable in a more extensive range as longer irradiation time and more intense UV irradiation are utilized for photo-induced releases. Therefore, the copolymer aggregates comprising ONBE-bearing DHGCs may have a great potential in photo-triggered drug delivery systems.

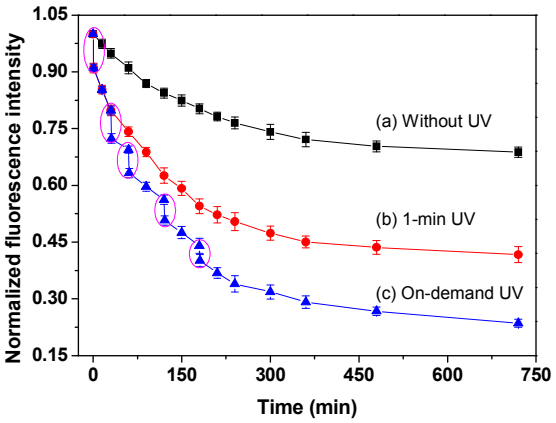

Fig. 10 *In vitro* release profiles of NR-loaded HG3 aggregates (c = 0.45 mg mL^{-1}) in PBS solution (50 mM, pH 7.4) at 37 °C with (b and c) or without (a) UV irradiation, in which the copolymer aggregates were subjected to 1-min light irradiation at the beginning of release process (b) or at each particular time of 0, 30, 60, 120 and 180 min (c, the circles were inserted to denote the drastic change of NFI before and after UV irradiation).

Conclusions

As a new subclass of hyperbranched-*graft*-linear copolymers, functional DHGCs were controllably synthesized by two step polymerizations involving RAFT SCVP and ROP. Hyperbranched PAP and PAP-*g*-PCL copolymers had relatively low polydispersity and controlled chemical composition, evident from ^{1}H NMR and GPC-MALLS analyses. Upon UV irradiation, hyperbranched PAP was converted into linear polymers, and PAP-*g*-PCL was readily degraded into mixtures of linear, star and graft polymers, which could be ascribed to the cleavage of ONBE functionality in each branching point. Amphiphilic HG3 could self-assemble into copolymer micelles in aqueous solution, which were gradually converted into vesicles and multicompartment vesicles with increasing UV irradiation time because of photo-induced cleavage and reaggregation of copolymer aggregates. Meanwhile, the release kinetics and cumulative release of Nile red from copolymer aggregates could be tuned in a wide range as normal and on-demand UV irradiations were applied, revealing the great potential in smart drug delivery systems. This study affords a general approach to construction of functional DHGCs and their derivatives, which can act as a versatile platform to explore the special properties and applications of novel macromolecular architecture in smart nanomaterials.

Acknowledgements

This work was financially supported by the National Natural Science Foundation of China (Grants 21274096 and 21474070), and the Project Funded by the Priority Academic Program Development of Jiangsu Higher Education Institutions.

Notes and references

[a] *Suzhou Key Laboratory of Macromolecular Design and Precision Synthesis, Jiangsu Key Laboratory of Advanced Functional Polymer Design and Application, College of Chemistry, Chemical Engineering and Materials Science, Soochow University, Suzhou 215123, China. Tel: +86-512-65882045; Fax: +86-512-65882045; E-mail: ylzhao@suda.edu.cn*

[b] *College of Textile and Clothing Engineering, Soochow University, Suzhou 215123, China*

† Electronic Supplementary Information (ESI) available: [^{1}H NMR, IR and fluorescence spectra, DLS plots, and results for photobleaching of Nile red]. See DOI: 10.1039/ b000000x/

1 C. Gao and D. Y. Yan, *Prog. Polym. Sci*., 2004, **29**, 183–275.
2 H. B. Jin, W. Huang, X. Y. Zhu, Y. F. Zhou and D. Y. Yan, *Chem. Soc. Rev*., 2012, **41**, 5986–5997.
3 B. I. Voit and A. Lederer, *Chem. Rev*., 2009, **109**, 5924–5973.
4 D. Wilms, S.-E. Stiriba and H. Frey, *Acc. Chem. Res*., 2010, **43**, 129–141.
5 C. Schüll and H. Frey, *Polymer*, 2013, **54**, 5443–5455.
6 A. Carlmark, E. Malmström and M. Malkoch, *Chem. Soc. Rev*., 2013, **42**, 5858–5879.
7 A. Carlmark, C. Hawker, A. Hult and M. Malkoch, *Chem. Soc. Rev*., 2009, **38**, 352–362.
8 D. Konkolewicz, M. J. Monteiro and S. Perrier, *Macromolecules*, 2011, **44**, 7067–7087.
9 R. Soleyman and M. Adeli, *Polym. Chem*., 2015, **6**, 10–24.
10 J. M. J. Fréchet, M. Henmi, I. Gitsov, S. Aoshima, M. R. Leduc and R. B. Grubbs, *Science*, 1995, **269**, 1080–1083.
11 Z. M. Wang, J. P. He, Y. F. Tao, L. Yang, H. J. Jiang and Y. L. Yang, *Macromolecules*, 2003, **36**, 7446–7452.
12 A. P. Vogt and B. S. Sumerlin, *Macromolecules,* 2008, **41**, 7368–7373.
13 M. J. Zhang, H. H. Liu, W. Shao, K. Miao and Y. L. Zhao, *Macromolecules*, 2013, **46**, 1325–1336.
14 S. P. Li and C. Gao, *Polym. Chem*., 2013, **4**, 4450–4460.
15 S. P. Li, J. Han and C. Gao, *Polym. Chem*., 2013, **4**, 1774–1787.
16 M. Rikkou-Kalourkoti, K. Matyjaszewski and C. S. Patrickios, *Macromolecules*, 2012, **45**, 1313–1320.
17 K. Matyjaszewski and N. V. Tsarevsky, *J. Am. Chem. Soc*., 2014, **136**, 6513–6533.
18 C. Pugh, A. Singh, R. Samuel and K. M. B. Ramos, *Macromolecules*, 2010, **43**, 5222–5232.
19 N. V. Tsarevsky, J. Y. Huang and K. Matyjaszewski, *J. Polym. Sci., Part A: Polym. Chem*., 2009, **47**, 6839–6851.
20 H. Sun, C. P. Kabb and B. S. Sumerlin, *Chem. Sci*., 2014, **5**, 4646–4655.
21 Y. Y. Zhuang, Q. Zhu, C. L. Tu, D. L. Wang, J. L. Wu, Y. M. Xia, G. S. Tong, L. He, B. S. Zhu, D. Y. Yan and X. Y. Zhu, *J. Mater. Chem*., 2012, **22**, 23852–23860.
22 Y. Y. Zhuang, Y. Su, Y. Peng, D. L. Wang, H. P. Deng, X. D. Xi, X. Y. Zhu and Y. F. Lu, *Biomacromolecules*, 2014, **15**, 1408–1418.
23 R. K. Kainthan, J. Janzen, E. Levin, D. V. Devine and D. E. Brooks, *Biomacromolecules*, 2006, **7**, 703–709.
24 D. Wilms, F. Wurm, J. Nieberle, P. Böhm, U. Kemmer-Jonas and H. Frey, *Macromolecules*, 2009, **42**, 3230–3236.
25 C. S. Popeney, M. C. Lukowiak, C. Böttcher, B. Schade, P. Welker, D. Mangoldt, G. Gunkel, Z. B. Guan and R. Haag, *ACS Macro Lett.*, 2012, **1**, 564–567.
26 C. Lach, R. Hanselmann, H. Frey and R. Mülhaupt, *Macromol. Rapid Commun.*, 1998, **19**, 461−465.
27 S. Pargen, J. Omeis, G. Jaunky, H. Keul and M. Möller, Macromol. *Chem. Phys*., 2011, **212**, 1791–1801.
28 A. Thomas, F. K. Wolf and H. Frey, *Macromol. Rapid Commun.*, 2011, **32**, 1910–1915.
29 P. L. Kuo, S. K. Ghosh, W. J. Liang and Y. T. Hsieh, *J. Polym. Sci. Part A: Polym. Chem.*, 2001, **39**, 3018–3023.
30 C. Schüll and H. Frey, *ACS Macro Lett.*, 2012, **1**, 461–464.
31 C. Schüll, L. Nuhn, C. Mangold, E. Christ, R. Zentel and H. Frey, *Macromolecules*, 2012, **45**, 5901–5910.
32 C. Schüll, H. Rabbel, F. Schmidand H. Frey, *Macromolecules*, 2013, **46**, 5823–5830.
33 M. Jesberger, L. Barner, M. H. Stenzel, E. Malmström, T. P. Davis and C. Barner-Kowollik, *J. Polym. Sci. Part A: Polym. Chem*., 2003, **41**, 3847–3861.

34 C. B. Zhang, Y. Zhou, Q. Liu, S. X. Li, S. Perrier and Y. L. Zhao, *Macromolecules*, 2011, **44**, 2034–2049.
35 M. J. Zhang, H. H. Liu, W. Shao, C. N. Ye and Y. L. Zhao, *Macromolecules*, 2012, **45**, 9312–9325.
36 J. Han, S. P. Li, A. J. Tang and C. Gao, *Macromolecules*, 2012, **45**, 4966–4977.
37 C. Xie, Z. H. Ju, C. Zhang, Y. L. Yang and J. P. He, *Macromolecules*, 2013, **46**, 1437–1446.
38 C. X. Li, H. H. Liu, D. D. Tang and Y. L. Zhao, *Polym. Chem.*, 2015, **6**, 1474–1486.
39 Y. Zhao, *Macromolecules*, 2012, **45**, 3647–3657.
40 J.-F. Gohy and Y. Zhao, *Chem. Soc. Rev*., 2013, **42**, 7117–7129.
41 Q. Yan, D. H. Han and Y. Zhao, *Polym. Chem*., 2013, **4**, 5026–5037.
42 H. Zhao, E. S. Sterner, E. B. Coughlin and P. Theato, *Macromolecules*, 2012, **45**, 1723–1736.
43 F. D. Jochum and P. Theato, *Chem. Soc. Rev.,* 2013, **42**, 7468–7483.
44 C. C. Zhu, C. Ninh and C. J. Bettinger, *Biomacromolecules*, 2014, **15**, 3474–3494.
45 D. R. Wang and X. G. Wang, *Prog. Polym. Sci*., 2013, **38**, 271–301.
46 G. Liu, W. Liu and C.-M. Dong, *Polym. Chem*., 2013, **4**, 3431–3443.
47 Y. Huang, R. J. Dong, X. Y. Zhu and D. Y. Yan, *Soft Matter*, 2014, **10**, 6121–6138.
48 L. Li, A. Lv, X.-X. Deng, F.-S. Du and Z.-C. Li, *Chem. Commun.,* 2013, **49**, 8549–8551.
49 Y. F. Zhang, Q. Yin, L. C. Yin, L. Ma, L. Tang and J. J. Cheng, *Angew. Chem. Int. Ed.,* 2013, **52**, 6435–6439.
50 L. L. Meng, W. Huang, D. L. Wang, X. H. Huang, X. Y. Zhu and D. Y. Yan, *Biomacromolecules*, 2013, **14**, 2601–2610.
51 A. Soleimani, A. Borecki and E. R. Gillies, *Polym. Chem*., 2014, **5**, 7062–7071.
52 J. Xuan, D. H. Han, H. S. Xia and Y. Zhao, *Langmuir*, 2014, **30**, 410–417.
53 Z.-Q. Yu, X.-M. Xu, C.-Y. Hong, D.-C. Wu and Y.-Z. You, *Macromolecules*, 2014, **47**, 4136–4143.
54 W. Z. Yuan and W. Guo, *Polym. Chem*., 2014, **5**, 4259–4267.
55 Q. Jin, T. J. Cai, H. J. Han, H. B. Wang, Y. Wang and J. Ji, *Macromol. Rapid Commun*., 2014*,* **35***,* 1372–1378.
56 G. Liu and C.-M. Dong, *Biomacromolecules,* 2012, **13**, 1573−1583.
57 G. Liu, L. Z. Zhou, Y. F. Guan, Y. Su and C.-M. Dong, *Macromol. Rapid Commun*., 2014*,* **35***,* 1673–1678.
58 Y. Zou, Y. Song, W. J. Yang, F. H. Meng, H. Y. Liu and Z. Y. Zhong, *J. Controlled Release*, 2014, **193**, 154–161.
59 O. Bertrand, E. Poggi, J.-F. Gohy and C.-A.Fustin, *Macromolecules,* 2014, **47**, 183–190.
60 C. G. Gamys, J.-M. Schumers, A. Vlad, C.-A. Fustin and J.-F. Gohy, *Soft Matter*, 2012, **8**, 4486–4493.
61 H. Zhao, W. Y. Gu, E. Sterner, T. P. Russell, E. B. Coughlin and P. Theato, *Macromolecules*, 2011, **44**, 6433–6440.
62 H. Zhao, W Y. Gu, R. Kakuchi, Z. W. Sun, E. Sterner, T. P. Russell, E. B. Coughlin and P. Theato, *ACS Macro Lett*., 2013, **2**, 966–969.
63 H. Zhao, W. Y. Gu, M. W. Thielke, E. Sterner, T. Tsai, T. P. Russell, E. B. Coughlin and P. Theato, *Macromolecules*, 2013, **46**, 5195–5201.
64 P. D. Haller, C. A. Flowers and M. Gupta, *Soft Matter*, 2011, **7**, 2428–2432.
65 L. Li, X.-X. Deng, Z.-L. Li, F.-S. Du and Z.-C. Li, *Macromolecules*, 2014, **47**, 4660–4667.
66 S. Chatterjee and S. Ramakrishnan, *Chem. Commun*., 2013, **49**, 11041–11043.
67 J. A. Barltrop, P. J. Plant and P. Schofield, *Chem. Commun*., 1966, **22**, 822–823.
68 A. Patchornik, B. Amit and R. B. Woodward, *J. Am. Chem. Soc*., 1970, **92**, 6333–6335.
69 C. P. Holmes and D. G. Jones, *J. Org. Chem*., 1995, **60**, 2318–2319.
70 X. Liu, Z. C. Tian, C. Chen and H. R. Allcock, *Polym. Chem*., 2013, **4**, 1115–1125.
71 J. Chiefari, Y. K. Chong, F. Ercole, J. Krstina, J. Jeffery, T. P. T. Le, R. T. A. Mayadunne, G. F. Meijs, C. L. Moad, G. Moad, E. Rizzardo and S. H. Thang, *Macromolecules*, 1998, **31**, 5559–5562.
72 Y. Mitsukami, M. S. Donovan, A. B. Lowe and C. L. McCormick, *Macromolecules,* 2001, **34**, 2248–2256.
73 P. Wu, M. Malkoch, J. N. Hunt, R. Vestberg, E. Kaltgrad, M. G. Finn, V. V. Fokin, K. B. Sharpless and C. J. Hawker, *Chem. Commun.*, 2005, 5775–5777.
74 M. R. Pavia, W. H. Moos and F. M. Hershenson, *J. Org. Chem.* 1990, **55**, 560–564.
75 A. P. Goodwin, J. L. Mynar, Y. Z. Ma, G. R. Fleming and J. M. J. Fréchet, *J. Am. Chem. Soc.*, 2005, **127**, 9952–9953.
76 X. Jiang, M. J. Zhang, S. X. Li, W. Shao and Y. L. Zhao, *Chem. Commun.,* 2012, **48**, 9906–9908.
77 W. Shao, K. Miao, H. H. Liu, C. N. Ye, J. Z. Du and Y. L. Zhao, *Polym. Chem*., 2013, **4**, 3398–3410**.**
78 K. Miao, W. Shao, H. H. Liu and Y. L. Zhao, *Polym. Chem*., 2014, **5**, 1191–1201.